

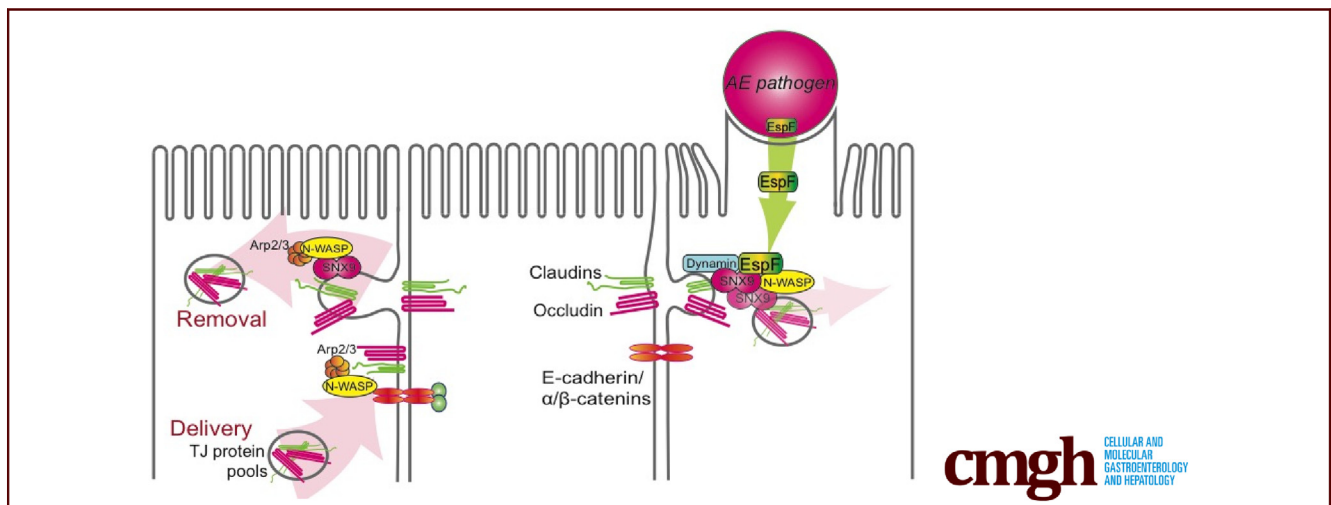
## ORIGINAL RESEARCH

## Attaching-and-Effacing Pathogens Exploit Junction Regulatory Activities of N-WASP and SNX9 to Disrupt the Intestinal Barrier



John J. Garber,<sup>1,2,3</sup> Emily M. Mallick,<sup>4</sup> Karen M. Scanlon,<sup>5</sup> Jerrold R. Turner,<sup>3,6</sup> Michael S. Donnenberg,<sup>5</sup> John M. Leong,<sup>7</sup> and Scott B. Snapper<sup>2,3,8</sup>

<sup>1</sup>Gastrointestinal Unit, Massachusetts General Hospital, Boston, Massachusetts; <sup>2</sup>Division of Gastroenterology/Nutrition and Center for Inflammatory Bowel Disease Treatment and Research, Boston Children's Hospital, Boston, Massachusetts; <sup>3</sup>Division of Gastroenterology and Hepatology, <sup>6</sup>Department of Pathology, Brigham and Women's Hospital, Boston, Massachusetts; <sup>3</sup>Department of Medicine, Harvard Medical School, Boston, Massachusetts; <sup>4</sup>Department of Medicine Microbiology and Physiological Systems, University of Massachusetts Medical School, Worcester, Massachusetts; <sup>5</sup>Department of Medicine and Department of Microbiology and Immunology, School of Medicine, University of Maryland, Baltimore, Maryland; <sup>7</sup>Department of Molecular Biology and Microbiology, Tufts University School of Medicine, Boston, Massachusetts



## SUMMARY

During enteric infection, the attaching-and-effacing pathogen virulence factor early secreted antigenic target-6 (ESX)-1 secretion-associated protein F (EspF) targets host Neural Wiskott-Aldrich Syndrome protein and sorting nexin 9 to promote junctional disruption and intestinal barrier loss. On this basis, we propose a novel role for the actin cytoskeletal regulatory protein Neural Wiskott-Aldrich Syndrome protein in controlling intestinal epithelial apical junction complex stability.

**BACKGROUND & AIMS:** Neural Wiskott-Aldrich Syndrome protein (N-WASP) is a key regulator of the actin cytoskeleton in epithelial tissues and is poised to mediate cytoskeletal-dependent aspects of apical junction complex (AJC) homeostasis. Attaching-and-effacing (AE) pathogens disrupt this homeostasis through translocation of the effector molecule early secreted antigenic target-6 (ESX)-1 secretion-associated protein F (EspF). Although the mechanisms underlying AJC disruption by EspF are unknown, EspF contains putative binding sites for N-WASP and the endocytic regulator sorting nexin 9 (SNX9). We hypothesized that

N-WASP regulates AJC integrity and AE pathogens use EspF to induce junctional disassembly through an N-WASP- and SNX9-dependent pathway.

**METHODS:** We analyzed mice with intestine-specific N-WASP deletion and generated cell lines with N-WASP and SNX9 depletion for dynamic functional assays. We generated EPEC and *Citrobacter rodentium* strains complemented with EspF bearing point mutations abolishing N-WASP and SNX9 binding to investigate the requirement for these interactions.

**RESULTS:** Mice lacking N-WASP in the intestinal epithelium showed spontaneously increased permeability, abnormal AJC morphology, and mislocalization of occludin. N-WASP depletion in epithelial cell lines led to impaired assembly and disassembly of tight junctions in response to changes in extracellular calcium. Cells lacking N-WASP or SNX9 supported actin pedestals and type III secretion, but were resistant to EPEC-induced AJC disassembly and loss of transepithelial resistance. We found that during *in vivo* infection with AE pathogens, EspF must bind both N-WASP and SNX9 to disrupt AJCs and induce intestinal barrier dysfunction.

**CONCLUSIONS:** Overall, these studies show that N-WASP critically regulates AJC homeostasis, and the AE pathogen

effector EspF specifically exploits both N-WASP and SNX9 to disrupt intestinal barrier integrity during infection. (*Cell Mol Gastroenterol Hepatol* 2018;5:273–288; <https://doi.org/10.1016/j.jcmgh.2017.11.015>)

**Keywords:** N-WASP; Cytoskeleton; Junction Regulation; EspF.

See editorial on page 420.

The apical junction complex (AJC), consisting of the tight junction (TJ) and adherens junction (AJ), is a multiprotein organelle that is intimately linked to dynamic networks of apical actin,<sup>1–3</sup> which, by simultaneously lending the AJC both stability and plasticity, enable it to control intestinal permeability. Neural Wiskott-Aldrich Syndrome protein (N-WASP) is a ubiquitously expressed protein that interacts with and activates the actin-related protein (Arp)2/3 complex, leading to robust polymerization of actin filaments. N-WASP has been shown to stabilize newly formed actin filaments and facilitate their incorporation into perijunctional rings critical for E-cadherin-dependent AJ stability.<sup>4</sup> There is also indirect evidence of a role for N-WASP in regulating both the delivery and removal of key junction proteins. A role for N-WASP in delivery of AJC proteins was suggested by studies in which chemical inhibition or depletion of N-WASP in epithelial cell lines was associated with defective delivery of occludin,<sup>5</sup> E-cadherin, and F-actin<sup>6</sup> to nascent AJCs. Evidence for N-WASP-mediated removal of AJC proteins comes from studies of *Drosophila* epithelium lacking Cell division cycle (Cdc)42, N-WASP, or Arp3. In these studies, genetic depletion of any member of the Cdc42/N-WASP/Arp pathway in fly epithelium led to defective internalization of E-cadherin and destabilization of the AJC.<sup>7,8</sup>

As the major regulator of intestinal permeability, the AJC is also the target of a number of bacterial pathogens, including enteropathogenic *Escherichia coli* (EPEC) and enterohemorrhagic *E coli* (EHEC), and the closely related mouse pathogen *Citrobacter rodentium*.<sup>9,10</sup> These pathogens use type III secretion to inject effector proteins that modulate a variety of host cellular processes. The first of these translocated proteins, the translocated intimin receptor (Tir), activates N-WASP, which results in localized actin polymerization and the formation of actin-rich pedestals and destruction of adjacent microvilli, lending this class of bacteria their designation as attaching-and-effacing (AE) pathogens.<sup>11</sup>

EPEC, EHEC, and *C rodentium* also disrupt intercellular junctions and induce intestinal barrier dysfunction,<sup>9,10</sup> and bacterial effector protein EspF, common to all 3 pathogens, has been shown to be required for AE pathogen-induced junction disruption.<sup>9</sup> Although the mechanism of EspF-mediated junction disruption remains unknown, EspF contains N-WASP binding sites and is capable of directly stimulating the actin polymerizing activity of N-WASP.<sup>12</sup> In addition to binding N-WASP, EspF also contains a nonoverlapping binding site for sorting nexin 9 (SNX9).<sup>12</sup> Sorting nexins are involved in diverse endocytic vesicle sorting activities, and the specific functions of SNX9 within the epithelium are largely unknown.<sup>13,14</sup> Direct binding of EspF to SNX9 alone appears to be

dispensable for mediating EspF-dependent TJ disruption,<sup>12</sup> although a role for EspF binding to N-WASP in mediating TJ disruption has not been reported.

We sought to evaluate the role that N-WASP, as a key regulator of actin dynamics, plays in maintaining AJC homeostasis, and to test whether AE pathogens, through EspF, exploit N-WASP-dependent pathways to disrupt AJC function. We first show in vivo and in vitro that N-WASP regulates AJC homeostasis, and is required for efficient TJ assembly and disassembly. Moreover, we identify a novel pathway whereby the bacterial effector EspF disrupts tight junctions through exploiting an otherwise homeostatic function of both N-WASP and SNX9 in regulating removal of TJ proteins from the AJC.

## Materials and Methods


### Mice

Mixed strain (Friend Virus B [FVB]/129) mice bearing a conditional *Wasl* knockout (KO) allele (*Wasl*<sup>flox/flox</sup>) were crossed with villin-Cre transgenic mice<sup>15</sup> to generate *Wasl*<sup>flox/flox</sup>; tg<sup>villin-Cre</sup> mice. Littermate *Wasl*<sup>flox/+</sup>; tg<sup>villin-Cre</sup> mice were used as controls in each experiment. Intestinal N-WASP KO (iNWKO) breeder mice and offspring were housed at either the Center for Comparative Medicine at the Massachusetts General Hospital or the Boston Children's Hospital animal facility. This study protocol was conducted in accordance with the Animal Research: Reporting of In Vivo Experiments (ARRIVE) guidelines and was approved by the animal ethics committees of both Massachusetts General Hospital and Boston Children's Hospital.

### Western Blot

For Western blot, intestinal epithelial cells were isolated from 8-week-old littermate control or iNWKO mice by EDTA dissociation as previously described,<sup>16</sup> and lysed with ice-cold buffer (150 mmol/L NaCl, 50 mmol/L Tris-HCl, pH 7.4, 1% Triton X-100 (Sigma, St. Louis, MO), complete protease inhibitor cocktail). Lysates were centrifuged at 13,000g for 15 minutes at 4°C and the supernatant (Triton-soluble cytoplasmic fraction) was collected. The pellet was resuspended in lysis buffer containing 1% sodium dodecyl sulfate and centrifuged, and the supernatant (Triton-insoluble

**Abbreviations used in this paper:** ADF, actin depolymerization factor; AE, attaching-and-effacing; AJ, adherens junction; AJC, apical junction complex; Arp, actin-related protein; CR, *Citrobacter rodentium*; Crb, Crumbs; DBS100, David B. Schauer 100; EcoRI, *E. coli* RY13 I; EHEC, enterohemorrhagic *Escherichia coli*; EM, electron microscopy; EPEC, enteropathogenic *Escherichia coli*; EspF, early secreted antigenic target-6 (ESX)-1 secretion-associated protein F; FITC, fluorescein isothiocyanate; iNWKO, intestine Neural Wiskott-Aldrich Syndrome protein knockout; KO, knockout; N-WASP, Neural Wiskott-Aldrich Syndrome protein; NWKD, Neural Wiskott-Aldrich Syndrome protein knockdown; PBS, phosphate-buffered saline; PCR, polymerase chain reaction; shRNA, short hairpin RNA; SNX9, sorting nexin 9; SNX9KD, sorting nexin 9 knockdown; TER, transepithelial electrical resistance; Tir, translocated intimin receptor; TJ, tight junction; ZO-1, zonula occludens-1.

 Most current article

© 2018 The Authors. Published by Elsevier Inc. on behalf of the AGA Institute. This is an open access article under the CC BY-NC-ND license (<http://creativecommons.org/licenses/by-nc-nd/4.0/>).

2352-345X

<https://doi.org/10.1016/j.jcmgh.2017.11.015>

membrane/cytoskeletal fraction) was collected. To assess short hairpin RNA (shRNA) knockdown in Caco-2 cells, monolayers were grown to approximately 90% confluence then lysed in ice-cold RIPA buffer (50 mmol/L Tris, 150 mmol/L NaCl, 0.1% sodium dodecyl sulfate, 0.5% sodium deoxycholate, 1% NP-40, protease inhibitors). Lysates were separated by sodium dodecyl sulfate gel electrophoresis, and transferred onto nitrocellulose membrane.<sup>16</sup> Immunoblotting was performed with rabbit polyclonal anti-N-WASP (1:2000) (kindly provided by Dr Marc Kirshner), or rabbit polyclonal anti-N-WASP antibody (1:500) (Cell Signaling Technology, Danvers, MA), followed by horseradish-peroxidase-conjugated goat anti-rabbit secondary antibody (1:3000; Cell Signaling), and visualized using enhanced chemiluminescence (GE Healthcare Life Sciences, Piscataway, NJ).

### *In Vivo Assessment of Intestinal Permeability*

The fluorescein isothiocyanate (FITC)-dextran assay was performed as previously described.<sup>17</sup> In brief, mice were administered 60 mg/100 g body weight 4 kilodaltons FITC-conjugated dextran (Sigma-Aldrich, St. Louis, MO) by oral gavage. Four hours later, whole blood was obtained by cardiac puncture in anesthetized animals and incubated on ice for 1 hour, followed by centrifugation at 13,000 rpm for 5 minutes to collect serum for assessment by direct fluorimetry.

### *Polarized Cell Culture*

Caco-2 brush border expressing (BBE) cells were obtained from the epithelial cell biology core at the Harvard Digestive Diseases Center. Cells were maintained in a humidified atmosphere of 5% CO<sub>2</sub> at 37°C, grown in Dulbecco's modified Eagle medium (Gibco Invitrogen, Paisley, UK) supplemented with 10% fetal bovine serum, 1% nonessential amino acids, 1% penicillin (1000 U/mL), and 1% streptomycin (1000 µg/mL). For permeability and infection studies, the cells were seeded on rat-tail collagen-coated 12-mm polycarbonate permeable Transwell cell culture inserts (0.4-µm pore size; Costar Corning, Inc, Corning, NY) at an initial density of 1 × 10<sup>4</sup> cells/well. Culture medium was replaced every 2–3 days as needed and cells were maintained for up to 31 days to form a differentiated monolayer. Cell confluence was confirmed by microscopic observance and measurement of transepithelial electrical resistance (TER) using a 12-well, 12-mm Endohm voltmeter (World Precision Instruments, Sarasota, FL) as previously described.<sup>18–20</sup>

### *shRNA Knockdown*

N-WASP and SNX9 knockdown were achieved by transducing Caco-2 cells with N-WASP shRNA (antisense sequence: GCTGGAGATACTTGTCAAG), SNX9 shRNA (antisense sequence: TACTCGTGATTACATCCATC), or scrambled control in a pLKO.1-based lentiviral vector (Open Biosystems, Pittsburgh, PA). After transduction, cells were selected and maintained in 10 µg/mL puromycin. N-WASP and SNX9 protein levels were determined after selection by Western blot and detection with rabbit polyclonal anti-N-WASP antibody (Cell Signaling Technology) and monoclonal mouse anti-SNX9 antibody (Abcam, Cambridge, MA).

Greater than 90% knockdown was confirmed by comparison of the optical density of N-WASP and SNX9 bands relative to tubulin loading controls in ImageJ software (National Institutes of Health, Bethesda, MD).

### *Line Scan and Kymographic Analysis*

Raw imaging stacks were analyzed using ImageJ software. A line 60-pixels long was drawn perpendicular to the junctional actin and a kymograph was created from the image sequence using the Multiple Kymograph and surface plot analysis functions of ImageJ software. For the line scan analysis, histogram data were saved as a text file and imported into Excel (Microsoft, Redmond, WA).

### *Generation and Passaging of Intestinal Organoids*

Small intestinal crypts were isolated from WT and iNWK0 mice and subsequently cultured to grow organoids according to the methods described by Miyoshi and Stappenbeck.<sup>21</sup> In brief, intestinal tissues were opened longitudinally and villi were removed by scraping with a glass coverslip before mincing and incubation in 2 mmol/L EDTA with gentle rocking. Supernatants obtained from successive incubations were examined to identify crypt-enriched fractions, which subsequently were maintained in basal culture medium consisting of advanced Dulbecco's modified Eagle medium/F12 supplemented with penicillin (100 U/mL) and streptomycin (100 mg/mL) (Life Technologies, Carlsbad, CA), GlutaMAX (Gibco, Gaithersburg, MD), and 10 mmol/L HEPES. Crypts were resuspended in Matrigel (Corning Life Sciences, Tewksbury, MA) at a density of 200 crypts/50 µL, and allowed to form hemispherical droplets by inversion at 37°C. After solidification of Matrigel droplets, 500 µL complete culture medium consisting of basal culture medium supplemented with B27 supplement (Life Technologies), 1 × N2 supplement (Life Technologies), 1 mmol/L N-acetyl-L-cysteine (Sigma-Aldrich), and 50% L-Wnt3A/R-spondin-3/noggin (WRN) conditioned media<sup>21</sup> was obtained from the Harvard Digestive Diseases Core. Organoids were passaged after 7–14 days in culture by gently breaking up the Matrigel by pipetting and resuspending organoids in 1 mL basal culture medium followed by gently disruption using a fire-polished Pasteur pipette. Organoids were washed with 10 mL basal culture medium to remove single and dead cells and resuspended in 50 µL Matrigel droplets, which were allowed to solidify before adding complete organoid media.

### *Antibodies and Immunofluorescence Microscopy*

Immunostaining was performed as previously described.<sup>22</sup> Briefly, for mouse intestinal tissue, 5-µm frozen sections were collected on coated slides, fixed in fresh 4% paraformaldehyde, and washed 3 times with phosphate-buffered saline (PBS) and permeabilized with 0.1% Triton-X 100. After incubation with anti-E-cadherin (Cell Signaling Technology), anti-occludin (Abcam), or anti-zonula occludens-1 (ZO-1) (Abcam) primary antibodies, all at 1:400, slides were washed and incubated with Alexa 594-conjugated goat anti-rabbit or Alexa 488-conjugated goat anti-rabbit secondary antibodies and DAPI (Life Technologies, Grand Island, NY). Standard epifluorescence microscopy was performed using an



AX70 upright microscope (Olympus, Tokyo, Japan). For polarized Caco-2 cells, the Transwell filters were cut out using a scalpel and immediately washed with PBS and fixed in 4% paraformaldehyde. Further staining was performed in 6- or 12-well plates as described for frozen sections. Confocal images were obtained with a Zeiss (Jena, Germany) Axiovert 200M microscope.

### Transmission Electron Microscopy

Electron microscopy (EM) was performed in the Microscopy Core in the Program for Membrane Biology at Massachusetts General Hospital. Intestinal tissues were fixed in 2.0% glutaraldehyde in 0.1 mol/L sodium cacodylate buffer (Electron Microscopy Sciences, Hatfield, PA) overnight at 4°C. The following day, samples were postfixed in 1.0% osmium tetroxide for 1 hour at room temperature, rinsed in buffer, and dehydrated through a graded series of ethanol. Samples then were infiltrated with Epon resin (Ted Pella, Redding, CA) in a 1:1 solution of Epon:ethanol overnight. The following day, they were placed in fresh Epon for several hours and then embedded in Epon overnight at 60°C. Thin sections were cut on a Leica (Wetzlar, Germany) EM UC7 ultramicrotome, collected on formvar-coated grids, stained with uranyl acetate and lead citrate, and examined in a JEOL (Peabody, MA) JEM 1011 transmission electron microscope at 80 kV. Images were collected at direct magnification of 30,000 $\times$  using an AMT digital imaging system (Advanced Microscopy Techniques, Danvers, MA).

### Calcium Switch

The calcium-switch technique has been described previously.<sup>23</sup> Briefly, for calcium depletion, once monolayers developed maximal TER, normal media was replaced with calcium-free Minimum Essential Medium Eagle Spinner Modification, which had been prewarmed to 37°C. Changes in TER were measured every 10 minutes for 1 hour. At 0-, 15-, and 30-minute time points, wells were harvested, washed in PBS, and fixed in fresh 4% paraformaldehyde for immunostaining as described earlier. For calcium repletion, fully confluent monolayers were cultured overnight in Minimum Essential Medium Eagle Spinner Modification, and the media replaced with complete Dulbecco's modified Eagle medium containing calcium. Serial TER measurements were obtained every 15 minutes for the first hour after calcium repletion, then every 30 minutes for 8 hours. At 0, 3, and 8 hours after calcium repletion, wells were harvested for junction characterization.

### Bacteria and Infections

For in vitro infections, wild-type EPEC strain E2348/69 (EPEC 0127:H7)<sup>24</sup> or E2348/69 (EspF) complemented with N-WASP- or SNX9-binding-defective EspF constructs (described later) were grown in Luria-Bertani broth with shaking at 37°C for 12 hours, and then maintained without shaking for 8 hours at 37°C to enhance type III secretion. For in vitro infections, bacterial density was assessed by photometric measurement of optical density (optical density of 600), and diluted to a final multiplicity of infection of 100 bacteria per cell in prewarmed Caco-2 medium without

antibiotics. Bacteria were allowed to adhere for up to 12 hours, and TER measurements were obtained at the indicated time points in triplicate wells. At 4 hours after infection, Transwell filters were removed and fixed in fresh 4% PFA for actin pedestal assessment and immunostaining. For in vivo infections, wild-type *C rodentium* strain David B. Schauer (DBS) 100, or DBS100 $\Delta$ espF (EM282) strains complemented with N-WASP- or SNX9-binding-defective EspF constructs were similarly grown overnight. Mice were infected by a single oral gavage of  $1 \times 10^9$  bacteria.

EspF-deficient EPEC strain UMD874 (E2348/69 $\Delta$ espF) has been described previously.<sup>25</sup> The EspF-deficient *C rodentium* strain EM282 (DBS100 $\Delta$ espF) was generated by using lambda red recombination.<sup>26</sup> Linear polymerase chain reaction (PCR) products containing the Zeocin cassette and its promoter region with flanking tails homologous to *C rodentium* espF were amplified from pDONR/Zeo. DBS100 containing pKD46, which carries the lambda red recombinase, was induced with arabinose to allow for expression of the lambda red recombinase. The linear PCR fragment then was electroporated into DBS100. Bacteria were recovered and plated on Zeocin to select for recombinants and deletions were confirmed by PCR.

### Generation of Modular EspF and N-WASP- and SNX9-Binding-Defective EspF

The modular version of EspF (pTM007) was generated by inverse PCR of pJN61 (a pTrc99A-based vector containing FLAG-tagged espF)<sup>27</sup> using the forward (GCCACGA ATTCCCAACCCGTCAGGCACCA) and reverse (CCGGAT GAATCCCCGGGAGTAAATGAAGTCACCTGGCTGCT) primers followed by *E. coli* RY13 I (EcoRI) digestion and ligation. This yielded a version of EspF that contained the N-terminal 73 amino acids, in addition to the third proline-rich region (PRR) and C-terminus (pTM001). The second PRR was amplified from pJN61 using the forward (GCCAACTCCGGAC CAACCCGTCGGGCACC) and reverse (CCGGATGAATCCCCGG GCTTAAAGCTTACAGTCTCAGACGCTT) primers and ligated into pCR-Blunt (pTM003). To generate a modular version of EspF that contained 2 PRR, pTM001 was linearized by *Xanthomonas malvacearum* I (XmaI) and EcoRI digestion, pTM003 was cut from pCR-Blunt by *Bacillus* sp. EI (BspEI) and EcoRI, and the 2 fragments were ligated. Performing XmaI and EcoRI digestion of the vector now containing 2 PRR, taking the BspEI/EcoRI digested pTM003 PRR and ligating the 2 fragments added a third PRR, yielding pTM007, a plasmid that contains the native N-terminus of EspF, 2 copies of the second PRR and the native third PRR and C-terminus. Point mutations that altered N-WASP (leucine 31 to alanine; L31A)<sup>28</sup> and SNX9 (arginine 3 to aspartic acid; R3D)<sup>12</sup> binding efficiencies were generated by Multi-site QuikChange Site-Directed Mutagenesis (Stratagene, La Jolla, CA) of pTM001 and pTM003 to ensure each PRR contained the nucleotide alterations before generating a version that contained multiple PRR. The N-WASP binding site was mutated using the forward (GCACAGGCA CTAAGATCATGCAGCTGCCTATGAGCAATCG) and reverse (CGATTGCTCATAGGCAGCTGCATGATCTTTTAGTGCCTGTGC) primers for pTM001, and the forward (CCATTGCACA

GGCATAAAAGATCATGCAGCTGCCTATGAACTATCG) and reverse (CGATAGTTCATAGGCAGCTGCATGATCTTTAATG CCTGTGCAATGG) primers for pTM003. The SNX9 binding site was mutated using the forward (CTCGGGGAATCCCA ACCGATCAGGCACCACCGCCACC) and reverse (GGTGGCGGT GGTGCCTGATCGTTGGAATTCCCGAG) primers for pTM001, and forward (CCAACCTCCGGACCAACCGATCCGG CACCGCCGCCACC) and reverse (GGTGGCGCGGTGCCGGA TCGGTTGGTCCGGAGTTGG) primers for pTM003.

### Data

All authors had access to the study data and reviewed and approved the final manuscript.

## Results

### Mice With Intestine-Specific N-WASP Deletion Have Spontaneous AJC Defects and Increased Intestinal Permeability

Germline deletion of N-WASP in mice results in early embryonic lethality.<sup>29</sup> To investigate the intestinal junction

regulatory functions of N-WASP in vivo, conditionally targeted *Wasl*<sup>fllox/fllox</sup> mice<sup>30–32</sup> were bred with mice expressing Cre recombinase under the intestine-specific promoter villin (*tg*<sup>vil-Cre</sup>).<sup>15</sup> iNWKO mice were viable and fertile, although tended to have lower overall average weights compared with littermate controls. H&E staining showed normal crypt-villous architecture with all epithelial cell lineages present and no evidence of spontaneous inflammation.<sup>32</sup>

Electron microscopic analysis showed that iNWKO mice displayed abnormal microvilli and decreased perijunctional actin (Figure 1A). Immunofluorescent staining showed normal junction localization of E-cadherin and ZO-1, but weak junction localization and more diffuse cytoplasmic staining of occludin (Figure 1B) despite comparable levels of total occludin protein in membrane and cytosolic fractions (Figure 1C). Although the pixel intensity by line scan at the tight junction appeared very similar between WT and N-WASP knockdown (NWKD) cells, the intensity of the occludin signal decreased more quickly as one moved away from the junction toward the cytoplasm in the WT cells

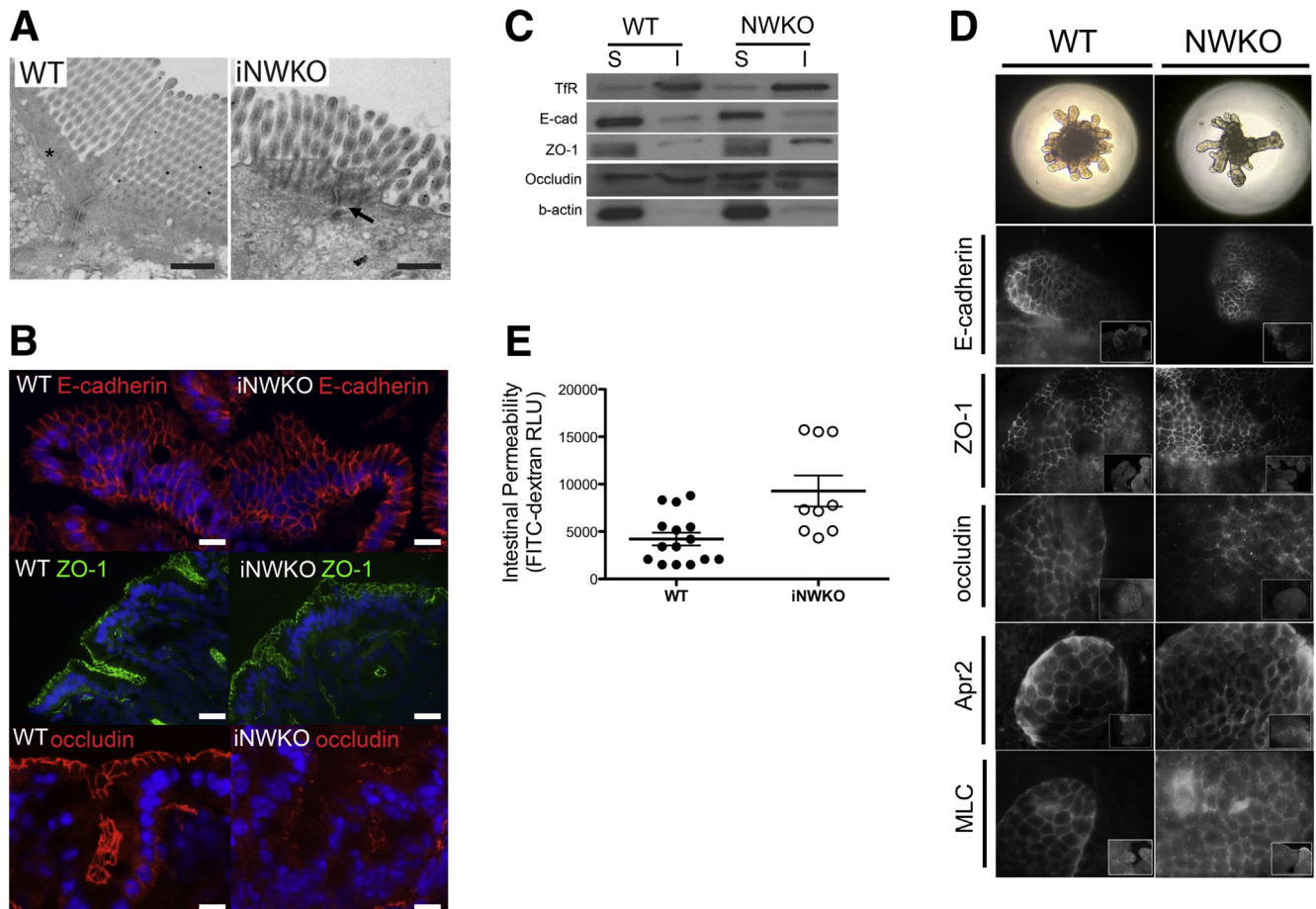


**Figure 1. Intestine-specific deletion of N-WASP leads to abnormalities in AJC morphology and function in vivo.** (A) Electron microscopic examination of small intestine iNWKO mice showing a lack of perijunctional actin (arrow) normally present in WT ileum (asterisk). (B) Immunofluorescence staining of E-cadherin (top), ZO-1 (middle), and occludin (bottom) in WT and iNWKO mice. (C) Occludin Western blot was similar between intestinal lysates from WT and iNWKO mice. (D) Small intestinal organoids generated from WT or iNWKO mice show normal patterns of E-cadherin, ZO-1, Arp2, and myosin light chain staining; organoids lacking N-WASP show decreased junction localization of occludin. (E) iNWKO mice showed significantly increased intestinal permeability by FITC-labeled dextran. Scale bars: (A) 500 nm; (B) 40  $\mu$ m. I, insoluble; RLU, relative light units; S, soluble.

compared with the NWKD cells, which reflects less discrete junctional staining in the absence of N-WASP. Decreased junction localization of occludin also was observed in N-WASP-deficient small intestinal organoids, whereas localization of other AJC-related proteins, including E-cadherin and ZO-1, as well as Arp2 and myosin light chain (MLC), were similar to WT controls (Figure 1D). To determine if abnormal junction localization of occludin observed in iNWKO mice and organoids correlated with impaired intestinal barrier function, we measured intestinal permeability and found spontaneously increased intestinal permeability to FITC-dextran in iNWKO mice when compared with littermate controls (Figure 1E). There were no significant differences in subcellular localization of Arp family members, including Arp2 and Arp3 (Figure 2A–C), or other AJC-related molecules including myosin light chain (Figure 2A–C) and claudin-1, -2, and -5 (Figure 2D).

### N-WASP Regulates Epithelial Permeability In Vitro

To investigate the mechanistic role(s) that N-WASP plays in regulating TJ dynamics, we generated

N-WASP-deficient Caco-2 cells (Figure 3A). When cultured on permeable Transwell filters, NWKD cells polarized normally and showed apical microvilli marked by phalloidin (Figure 3B, left) and well-defined junction complexes marked by E-cadherin (Figure 3B, right). In contrast to E-cadherin and ZO-1 (Figure 3C, top and bottom), the junctional localization of occludin was less distinct with more cytoplasmic staining in NWKD cells (Figure 3C, middle). By using line scan analysis,<sup>33</sup> we found no quantitative differences in E-cadherin or ZO-1 localization at the AJC between WT and NWKD cells (Figure 3D, top and bottom). In contrast, the occludin signal was diminished at intercellular junctions in NWKD cells when compared with WT cells and was more pronounced in the cytoplasm (Figure 3D, middle).

To next assess whether the aberrant TJ morphology correlated with altered barrier function, we measured the development of TER over the course of 30 days after seeding on permeable Transwell filters and found that the maximal TER achieved by fully polarized NWKD cells was ultimately 25% less than cells expressing normal levels of N-WASP (Figure 3E). Of note, NWKD cells developed TER more rapidly around days 12–13, which may reflect slightly

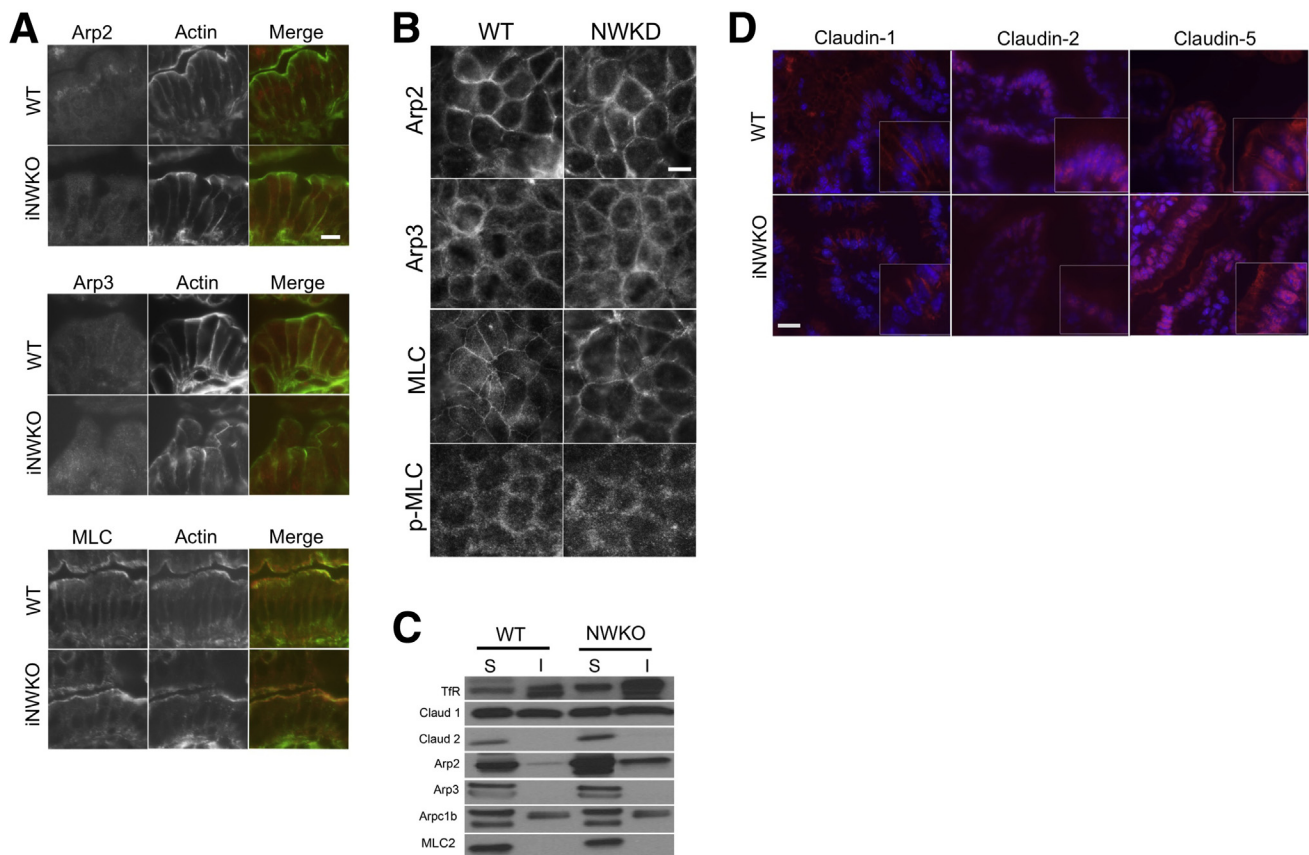


**Figure 2. N-WASP depletion does not affect Arp2/3, MLC, or claudin-1, -2, and -5.** (A and B) Immunolocalization showed normal patterns of Arp2, Arp3, and MLC in iNWKO mice and NWKD cells. (C) Western blot for Triton-soluble (S) cytoplasmic fraction and Triton-insoluble (I) membrane/cytoskeletal fractions of primary intestinal epithelial lysates did not show any significant differences in key AJC proteins, including Arp complex proteins, claudin-1 and -2, and MLC in WT and iNWKO mice. (D) Immunolocalization showed similar patterns of claudin-1, -2, and -5 in iNWKO and WT control mice. Scale bars: (A and D) 20  $\mu\text{m}$ ; (B) 5  $\mu\text{m}$ .



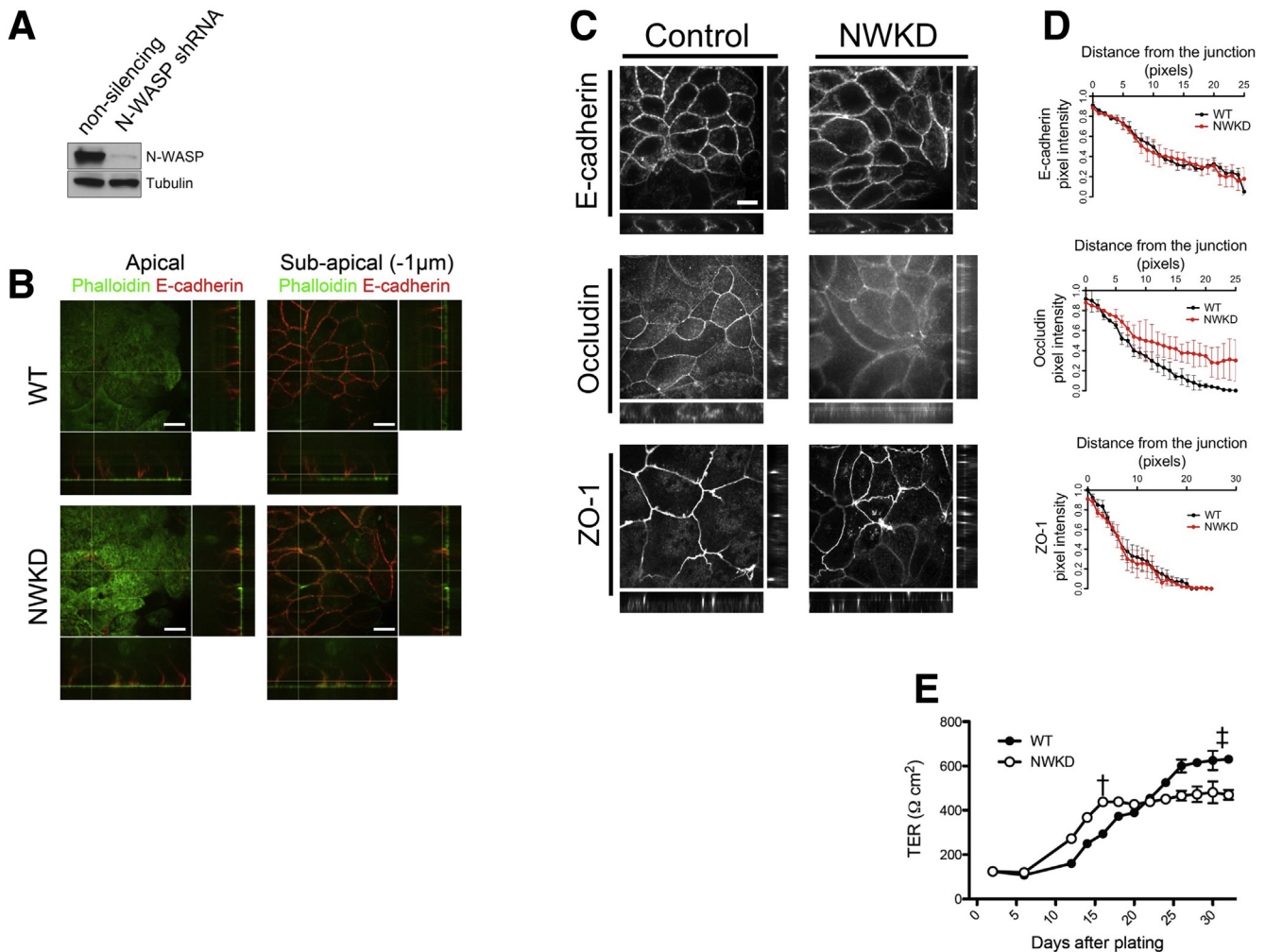


**Figure 3. N-WASP depletion leads to junction abnormalities and increased permeability in vitro.** (A) Western blot showing >90% knockdown of N-WASP using N-WASP-specific shRNA. (B) NWKD cells polarized normally and showed apical microvilli marked by phalloidin (*left*) and well-defined junction complexes marked by E-cadherin (*right*). (C) Immunolocalization of junction proteins showed normal patterns of E-cadherin (*top*) and ZO-1 (*middle*), while occludin (*bottom*) was less concentrated at cell junctions and displayed more cytoplasmic staining in NWKD cells. (D) In both WT and NWKD monolayers, E-cadherin and ZO-1 pixel density was tightly focused at the AJC, with very little cytoplasmic signal; occludin pixel intensity was less concentrated at intercellular junctions in NWKD monolayers. (E) NWKD monolayers developed TER more quickly (*f*) during the first 14 days, but had an overall lower maximal steady-state TER compared with WT monolayers ( $\dagger P < .05$ ). (B and C) Scale bars: 5  $\mu$ m.

increased proliferation and more rapid confluency in NWKD monolayers, but TER essentially plateaued and did not significantly increase beyond day 14 in culture.

To determine whether N-WASP influences the ability of the AJC to dynamically alter permeability in response to exogenous signals, we used the calcium-switch technique, in which removal of calcium from the culture medium of mature monolayers rapidly induces junction disassembly and loss of TER, and restoring calcium promotes junction reassembly and recovery of TER.<sup>23</sup> Consistent with a role for N-WASP in internalization of AJC proteins, N-WASP depletion led to a delayed response during calcium withdrawal compared with WT controls: 10 minutes after calcium removal, WT monolayers showed a 27.6% loss of TER (range, 17.7%–36.9%), whereas TER in NWKD monolayers was essentially unchanged from its starting value

(99.6%–104%;  $P < .05$  vs WT), and took approximately twice as long to reach a similar decrement (28% decrease in TER after 19.4 minutes) (Figure 4A). Delayed junction disassembly in NWKD cells also was reflected by the persistence of well-formed tight junctions, with increased persistence of occludin, but not E-cadherin or F-actin, in NWKD cells compared with WT control cells during calcium depletion (Figure 4B).

N-WASP depletion also resulted in delayed junction reassembly. After overnight culture in low-calcium medium, we performed serial TER measurements in WT and NWKD cultures after restoring calcium to the media. Recovery of TER in NWKD cells significantly lagged behind that of WT: although WT cells rapidly recovered monolayer resistance between 2 and 6 hours after calcium repletion, TER in NWKD cultures only gradually began to increase

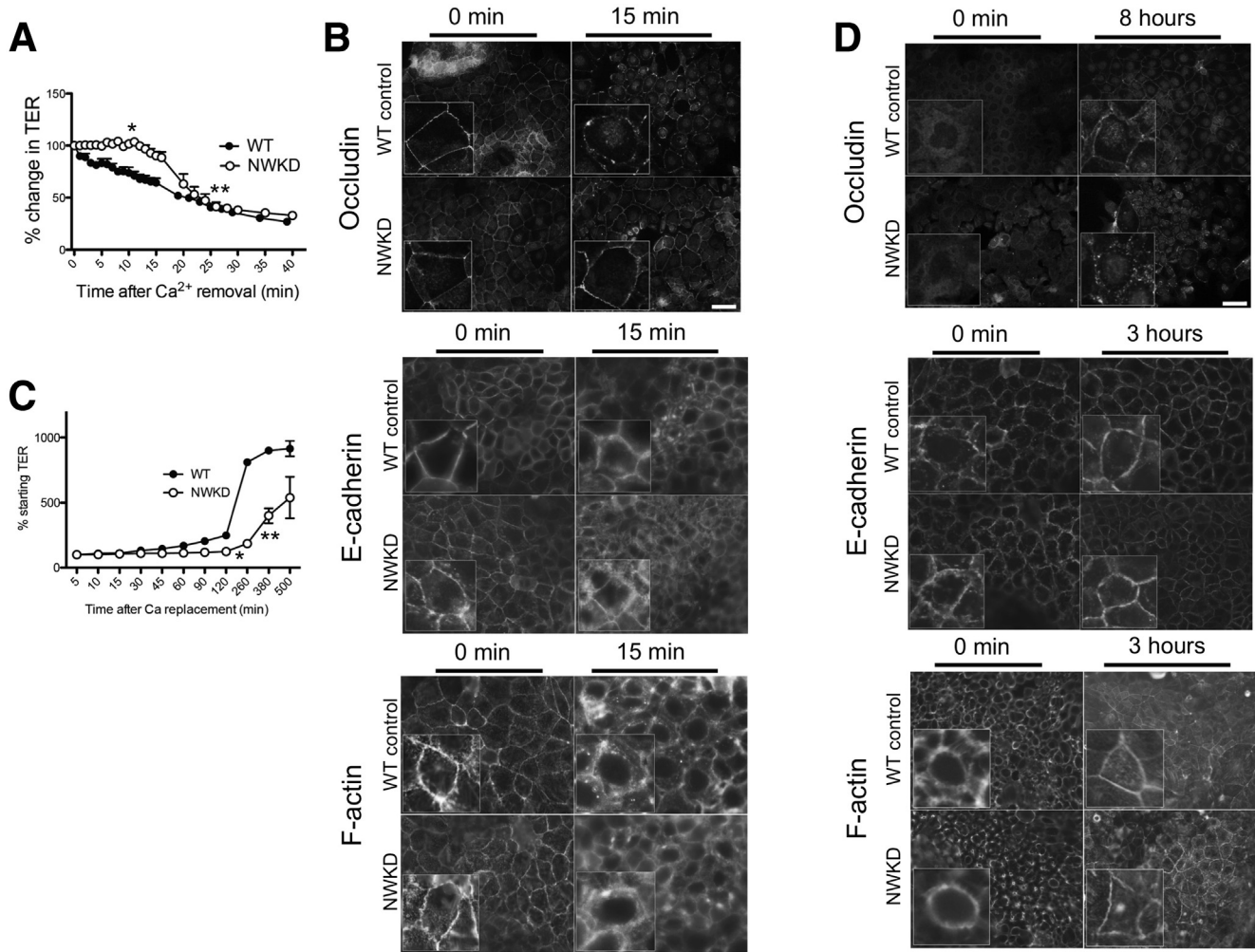


**Figure 4. Calcium-switch shows delayed junction dynamics in N-WASP-depleted cells.** (A) TER measurements in WT and NWKD monolayers subjected to calcium depletion. After 10 minutes, WT cells lost approximately 30% of initial TER, whereas TER was essentially unchanged in NWKD cells at the same time point (*asterisk*), and did not decrease to the same degree as in WT cells until >25 minutes after calcium removal (*double asterisk*). (B) Delayed junction disassembly in NWKD cells was reflected by the persistence of occludin, but not E-cadherin or F-actin, in NWKD cells compared with WT control cells 15 minutes after calcium depletion. (C) Serial TER measurements in WT and NWKD monolayers during calcium repletion. Recovery of TER in NWKD monolayers significantly lagged behind WT cultures (*asterisk* and *double asterisk*). (D) Occludin remained primarily localized to the cytoplasm in NWKD cultures at 8 hours (*top panel*). In contrast to the effects observed for occludin, junction localization of E-cadherin and F-actin appeared similar in calcium-repleted NWKD and control monolayers (*lower panels*). (B and D) Scale bars: 10  $\mu$ m.

after 2 hours, and did not return to steady-state TER until after >8 hours (Figure 4C). The delay in TER recovery induced by N-WASP depletion also correlated with delayed recovery of AJC morphology. Although both WT and NWKD cells displayed a complete disruption of occludin localization after overnight culture in low-calcium media (Figure 4D, left panels), the majority of occludin signal relocalized to the cell-cell junctions in WT cells 8 hours after restoring calcium to the culture medium. In contrast, occludin remained primarily localized to the cytoplasm in NWKD cultures at 8 hours (Figure 4D, top panel). In contrast to the effects observed for occludin, junction localization of E-cadherin and F-actin appeared similar in calcium-repleted NWKD and control monolayers (Figure 4D, lower panels).

#### Host N-WASP and SNX9 Are Required for EPEC-Induced Barrier Dysfunction and Junction Disruption

Because EspF, an AE pathogen effector protein essential for TJ disruption, is capable of binding both N-WASP and the endocytic modulator SNX9,<sup>12</sup> we hypothesized that EspF induces intestinal barrier dysfunction by simultaneously activating N-WASP and SNX9 to stimulate the internalization of AJC proteins. We first assessed the ability of WT EPEC,<sup>24</sup> expressing native EspF, to induce TJ disruption and permeability changes. After 4 hours of infection, EPEC induced a 61.4% decrease in TER (range, 51%–72%) in WT monolayers, whereas NWKD monolayers were more resistant to barrier disruption, with TER decreasing by 28.8%



(range, 25%–34%’  $P < .01$  for  $\Delta$ TER in NWKD vs WT) (Figure 5A). As expected,<sup>11,34,35</sup> membrane-attached EPEC induced robust actin pedestal formation on WT cells (Figure 5B and C), along with the relocalization of ZO-1 to the tip of actin pedestals (Figure 5B, white arrows). Somewhat unexpectedly, EPEC also was able to induce pedestals on NWKD cells (Figure 5B, second row), but despite the presence of a large number of actin pedestals, did not disrupt ZO-1 or E-cadherin, or induce the relocalization of these AJC proteins to actin pedestals in the setting of reduced N-WASP levels. Apical (XY plane) views showed strong staining of both E-cadherin and ZO-1 at the periphery between neighboring EPEC-infected NWKD cells, and side views (XZ and YZ planes) showed well-defined linear

strands of both AJC proteins (Figure 5B and C). In contrast, ZO-1 was not localized at junctions in EPEC-infected WT cells (Figure 5B, top row). Consistent with these findings, surface intensity plots of ZO-1 pixel distribution derived from cell–cell boundaries showed reduced peak intensities in EPEC-infected WT, but not NWKD, cells (data not shown), indicating inefficient TJ disruption in the absence of N-WASP.

Each PRR from EspF has nonoverlapping binding sites for both N-WASP and SNX9, suggesting that the ability to simultaneously interact with both of these host proteins may be important for the maximal activity of EspF.<sup>12</sup> To investigate whether SNX9, similar to N-WASP, was required for EPEC-induced junction disruption, we

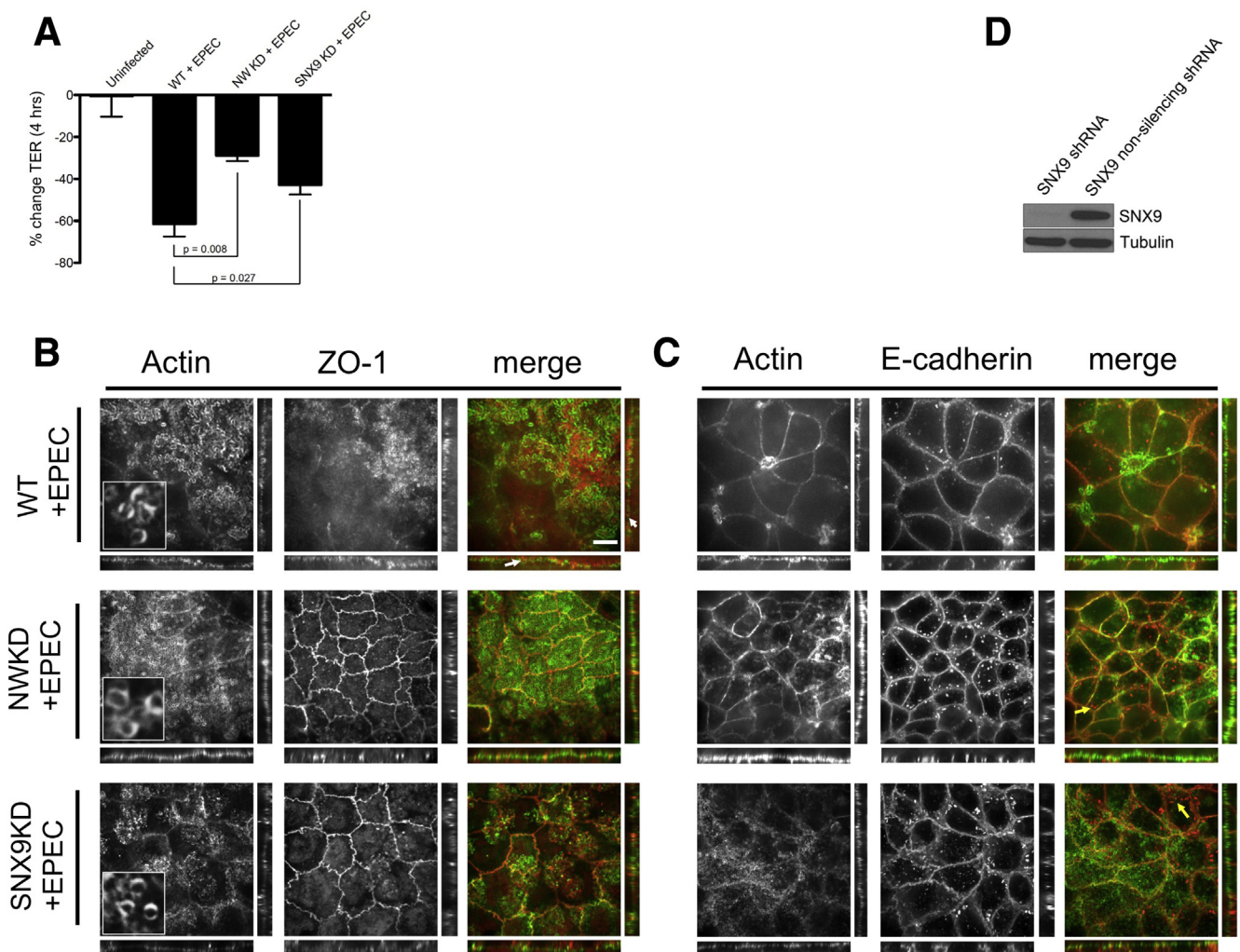


**Figure 5. N-WASP and SNX9 are required for EspF-mediated junction disruption during infection with EPEC.** (A) Change in TER after 4 hours of EPEC infection in NWKD or SNX9 cells. (B and C) Confocal immunofluorescence of WT, NWKD, and SNX9KD monolayers infected with EPEC. Both NWKD (middle row) and SNX9KD (bottom row) cells supported robust actin-pedestal formation during EPEC infection (actin pedestals on higher-magnification insets), comparable with WT cells, but although EPEC disrupted the normal localization of ZO-1 with re-localization to the pedestal (upper row, white arrows) in WT cells, junctional localization of E-cadherin and ZO-1 was essentially preserved in both NWKD and SNX9KD cells. Orthogonal views (to the right and below each main panel) also showed preserved linear strands of E-cadherin and ZO-1 in NWKD and SNX9KD cells whereas linear strands of ZO-1 were lost in EPEC-infected WT cells. In NWKD and SNX9KD, there were numerous cytoplasmic perijunctional puncta enriched for E-cadherin (yellow arrows), which were rarely observed in infected WT cells. (D) Western blot confirming efficient knockdown of SNX9 protein using shRNA. Scale bars: 10  $\mu$ m.

generated Caco-2 cell lines with stable SNX9 knockdown (SNX9KD) (Figure 5D). Similar to the NWKD cells, SNX9KD cells were partially resistant to EPEC-induced permeability changes, with TER decreasing by 43.7% (range, 22%–58%;  $P < .05$  for  $\Delta$ TER in SNX9KD vs WT) after 4 hours in EPEC-infected SNX9KD cells, compared with a 61.4% decrease in TER (range, 51%–72%) in WT cells (Figure 5A). After 4 hours, EPEC-infected SNX9KD cells showed a large number of actin pedestals and loss of the brush border (Figure 3B, bottom row), however, similar to NWKD cells, E-cadherin and ZO-1 retained their discrete junctional localization patterns without relocation of ZO-1 to actin pedestals (Figure 5B and C, bottom rows). Of note, both NWKD and SNX9KD cells showed numerous cytoplasmic perijunctional puncta (mean, 4.08/cell  $\pm$  0.41 SEM for NWKD; 4.26/cell  $\pm$  0.47 SEM for SNX9KD), which were enriched for E-cadherin but not ZO-1 (Figure 5C, yellow arrows), which may represent vesicles in an E-cadherin-specific

recycling pathway that have accumulated owing to impaired efficiency of endocytosis in the absence of N-WASP or SNX9.

### EspF Requires Both N-WASP and SNX9 Binding to Induce Efficient Relocalization of TJ Proteins

We next sought to determine whether EPEC strains expressing EspF variants that are unable to bind either N-WASP or SNX9 are able to induce epithelial barrier dysfunction. We introduced point mutations in each of the 3 C-terminal PRR repeats in either the N-WASP (L31A) or SNX9 (R3D) binding domains of *espF* (Figure 6A), previously shown to be important for binding to N-WASP and SNX9.<sup>12</sup> We then complemented the EspF-deficient EPEC strain UMD874 (E2348/69 $\Delta$ *espF*) with N-WASP-binding-defective EspF (pEspF<sub>NWBD</sub>) or SNX9-binding-defective EspF (pEspF<sub>SNX9BD</sub>), generating EPEC $\Delta$ *espF*/pEspF<sub>NWBD</sub> and EPEC $\Delta$ *espF*/

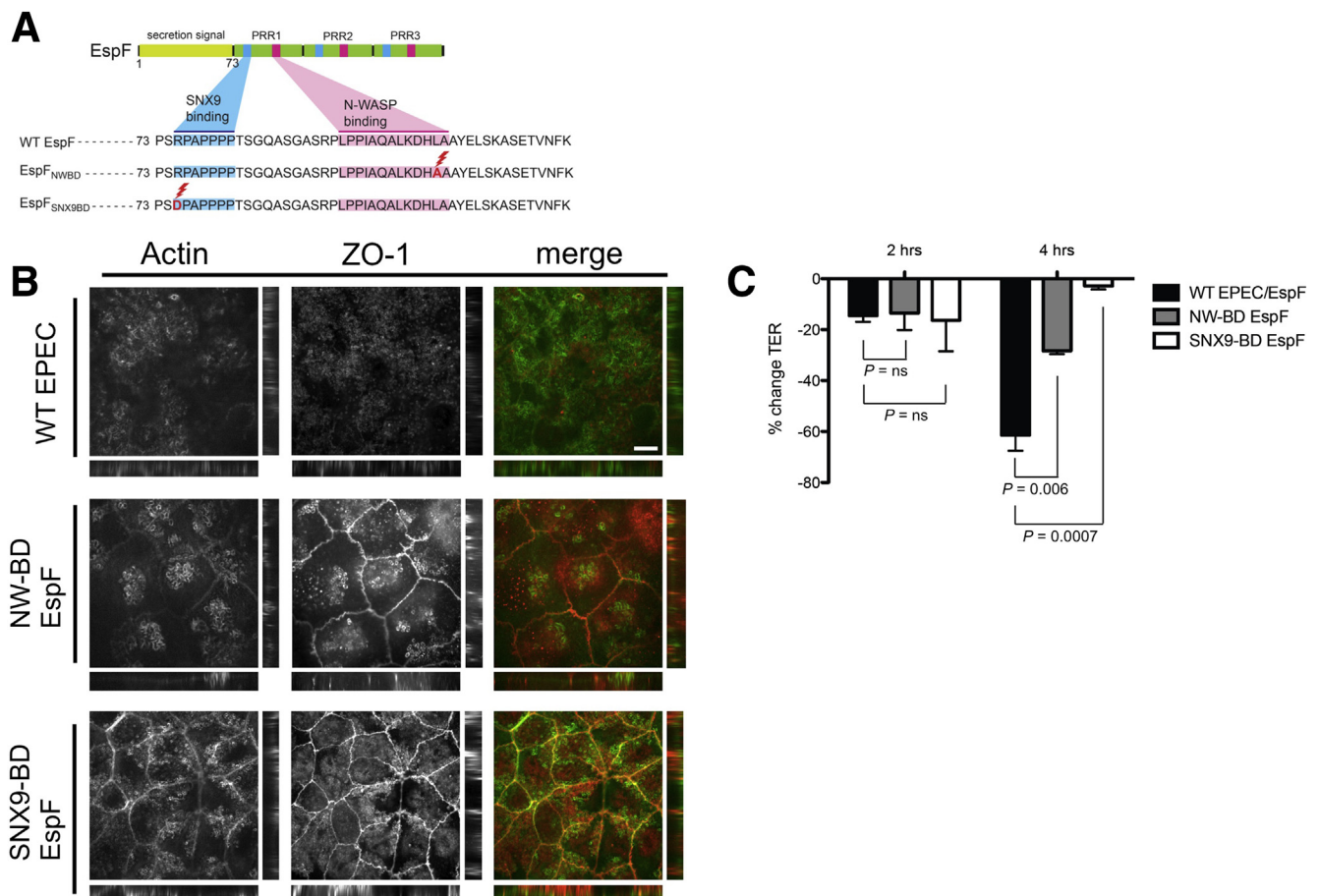


**Figure 6. Mutations in N-WASP- and SNX9-binding regions of EspF attenuate EPEC-induced junction disruption in vitro.** (A) Schematic of point mutations made in each PRR of EspF, rendering it unable to bind to N-WASP or SNX9. (B) WT EPEC induced robust actin pedestal formation, disruption of ZO-1 localization, and recruitment of ZO-1 to the tips of actin pedestals; in contrast, EPEC $\Delta$ *espF*/pEspF<sub>NWBD</sub> and EPEC $\Delta$ *espF*/pEspF<sub>SNX9BD</sub> were both attenuated in their ability to induce TJ disruption, with persistent junction localization of ZO-1 (arrowheads) in infected cells. (C) WT cells infected with EPEC expressing WT EspF showed a 61.4% reduction in TER at 4 hours after infection; in contrast, EPEC $\Delta$ *espF*/pEspF<sub>NWBD</sub> was only able to induce a 28.4% reduction in TER, and there was minimal change in TER at 4 hours in monolayers infected with EPEC $\Delta$ *espF*/pEspF<sub>SNX9BD</sub> ( $P < .01$  for WT EPEC vs EPEC $\Delta$ *espF*/pEspF<sub>NWBD</sub>;  $P < .01$  for WT EPEC vs EPEC $\Delta$ *espF*/pEspF<sub>SNX9BD</sub>). Scale bars: 10  $\mu$ m.



pEspF<sub>SNX9BD</sub>, respectively. WT cells infected with EPEC expressing WT EspF showed a 61.4% reduction in TER at 4 hours after infection; in contrast, EPEC $\Delta$ espF/pEspF<sub>NWBD</sub> was only able to induce a 28.4% reduction in TER, and there was minimal change in TER at 4 hours in monolayers infected with EPEC $\Delta$ espF/pEspF<sub>SNX9BD</sub> ( $P < .01$  for WT EPEC vs EPEC $\Delta$ espF/pEspF<sub>NWBD</sub>;  $P < .01$  for WT EPEC vs EPEC $\Delta$ espF/pEspF<sub>SNX9BD</sub>) (Figure 6C). Both EPEC $\Delta$ espF/pEspF<sub>NWBD</sub> and EPEC $\Delta$ espF/pEspF<sub>SNX9BD</sub> were impaired in their ability to induce tight junction disruption, and ZO-1 remained discretely localized in subapical linear strands at the junction without relocalizing to actin pedestals (Figure 6B). Together, these results show that EspF specifically targets and disrupts tight junctions, and binding to both host N-WASP and SNX9 are required for its full activity.

### *C. rodentium* EspF Must Bind Both N-WASP and SNX9 to Induce Intestinal Pathology In Vivo

To test whether N-WASP and SNX9 binding are important for the pathogenicity of AE bacteria in vivo, we

generated a *C. rodentium* (CR) strain lacking EspF, and complemented this with N-WASP- or SNX9-binding-defective EspF constructs. WT mice were infected with a single dose of  $5 \times 10^8$  colony-forming units WT CR, CR $\Delta$ espF, CR $\Delta$ espF/pEspF<sub>NWBD</sub>, or CR $\Delta$ espF/pEspF<sub>SNX9BD</sub> and followed up for 7 days. We first confirmed that WT CR could efficiently colonize WT mice and noted numerous actin pedestals and AE lesions in WT, but not iNWKO, mice by EM (Figure 7A, arrows). As previously described,<sup>36,37</sup> mice infected with WT CR lost weight (Figure 7B) and shed high titers of CR in the stool throughout the first 7 days of infection (Figure 5C). In contrast, disease was attenuated in mice infected with isogenic CR $\Delta$ espF strains expressing variant EspF unable to bind either N-WASP or SNX9. Mice infected with CR $\Delta$ espF/pEspF<sub>NWBD</sub> or CR $\Delta$ espF/pEspF<sub>SNX9BD</sub> did not lose weight (Figure 7B). Both the WT and mutant CR strains were able to efficiently colonize mice (Figure 7C). Consistent with previous reports,<sup>9</sup> CR expressing WT EspF induced marked disruption of junction localization of ZO-1 (Figure 7D, upper right). In contrast, and despite the presence of at least  $10^7$  colony-forming

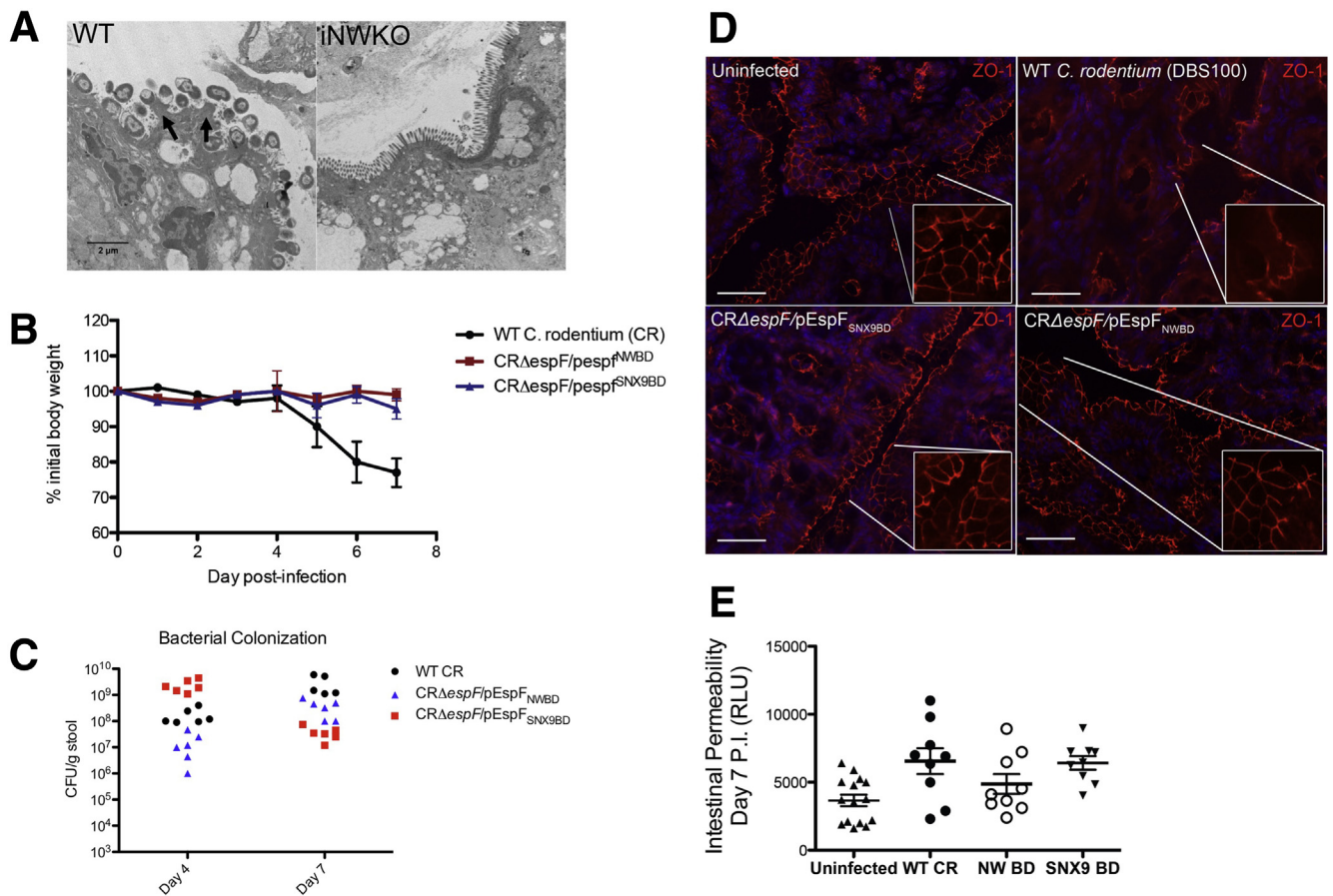


**Figure 7. Mutations in N-WASP- and SNX9-binding regions of EspF attenuate CR-induced junction disruption in vivo.** (A) WT CR induced robust actin-dense pedestal formation in WT, but not iNWKO mice. (B) WT mice infected with WT CR (black line), but not CR complemented with N-WASP- or SNX9-binding-defective EspF (red and blue lines, respectively), showed weight loss during acute infection. (C) Bacterial colonization by WT CR, CR $\Delta$ espF/pEspF<sub>NWBD</sub> and CR $\Delta$ espF/pEspF<sub>SNX9BD</sub>. (D) CR expressing wild-type EspF induced marked disruption of normal ZO-1 patterns by 7 days after infection (upper right); in contrast, CR $\Delta$ espF strains complemented with N-WASP or SNX9-binding-defective EspF failed to disrupt localization of ZO-1 at intercellular junctions. (E) Loss of EspF binding to host N-WASP (CR $\Delta$ espF/pEspF<sub>NWBD</sub>) attenuates increases in intestinal permeability to FITC-dextran induced by CR during in vivo infection. Scale bars: 20  $\mu$ m. RLU, relative light unit.



units/g of stool CR, the strains complemented with N-WASP- and SNX9-binding-defective EspF constructs were unable to induce AJC disruption, and ZO-1 appeared essentially unaffected (Figure 7D, bottom panels). Attenuation in the ability of CR expressing N-WASP-binding-defective EspF also correlated with protection from pathogen-induced increases in intestinal permeability to FITC-dextran compared with mice infected with WT CR (Figure 7E).

## Discussion

In the intestinal epithelium, the AJC is intimately linked to dynamic networks of actin, and the ability of N-WASP to rapidly catalyze actin polymerization makes it an ideal candidate for controlling junction protein mobilization and turnover, which may ultimately influence AJC permeability. We found that mice lacking N-WASP in the intestinal epithelium have abnormal junction morphology and increased intestinal permeability. These findings correlate with the absence of perijunctional actin and a terminal web, in association with mislocalization of occludin.

We considered several ways in which N-WASP function might influence dynamic AJC states, including facilitating either the delivery or removal of AJC proteins, and found that N-WASP is required for both the efficient assembly and disassembly of the AJC in response to conditions that induce rapid cell depolarization and repolarization. The Arp2/3 complex, for which N-WASP is a key nucleation-promoting factor, has been shown to play an important role in endocytic vesicle organization and trafficking, and enterocytes from mice with intestine-specific ArpC3 deletion show extensive vesiculation and inclusions.<sup>38</sup> Notably, ArpC3 deletion does not affect the formation of early endosomes, but leads to prominent mislocalization of Vacuolar Protein Sorting (VPS) 26, a subunit of the retromer complex that participates in cargo loading into membrane tubules coated by Phox homology (PH)-BIN1, Amphiphysin and RVS167 (BAR) proteins, including multiple members of the sorting nexin protein family.<sup>39-41</sup> The potential importance of actin cytoskeleton-mediated endocytosis in controlling AJC homeostasis is highlighted further by studies showing that intestinal deletion of cortactin, a dynamin-interacting protein that recruits Arp2/3 proteins to existing actin filaments, leads to reduced junction levels of ZO-1, claudin-1, and E-cadherin, and increased epithelial permeability.<sup>42</sup> The N-WASP-Arp2/3 complex therefore may directly promote TJ protein endocytosis, even in the absence of infection, through interacting with additional host proteins important for endocytosis, such as retromer complex and sorting nexin proteins as well as cortactin. Such a complex would spatially and temporally unite the molecular machinery necessary to generate propulsive forces that drive both vesicle elongation/detachment (N-WASP-mediated actin assembly), as well as the energy necessary for membrane scission and internalization of AJC-protein-containing vesicles (via SNX9 and dynamin).

An important concept in dynamic actin cytoskeletal regulation central to many homeostatic processes is actin

filament treadmilling, in which actin polymerization is counterbalanced with depolymerization, and the relative contributions of these closely linked processes enables actin filaments to generate propulsive forces and serve as dynamic structural scaffolds.<sup>43</sup> The N-WASP-Arp2/3 complex primarily promotes polymerization of actin filaments and the formation of branched-actin-filament networks, whereas actin depolymerization factor (ADF) family proteins (ADF, cofilin-1, cofilin-2) severs and disassembles existing filaments, an activity that is significantly enhanced by the cofactor actin-interacting protein 1.<sup>44-46</sup> Notably, several recent studies have suggested a key role for ADF/cofilin-1 in regulating the remodeling and permeability of epithelial junctions because loss of either cofilin-1, ADF, or actin-interacting protein 1 was associated with increased epithelial permeability, delayed AJC assembly, and increased susceptibility to dextran sodium sulfate-induced colitis.<sup>47,48</sup> Although ADF/cofilin proteins primarily promote depolymerization during actin treadmilling, the activity of ADF/cofilin on existing filaments produces free barbed ends for subsequent Arp2/3 filament nucleation, and the overall result may be to promote N-WASP-Arp2/3-dependent actin polymerization, in which newly polymerized actin filaments are more stable than on older filaments.<sup>49</sup> Therefore, in addition to defects in AJC protein endocytosis, loss of N-WASP in the intestinal epithelium also may disrupt the critical balance of actin polymerization and depolymerization by failing to nucleate new actin filaments at ADF/cofilin-produced free barbed ends. The overall result may be defective perijunctional force-generating polymer motors and protein scaffolds leading to increased permeability and impaired dynamic AJC assembly and disassembly.

The significance of cytoskeletal regulation and its relationship to intestinal barrier maintenance also is highlighted by enteric pathogens that specifically target host proteins, including N-WASP, as part of their pathogenic strategy. EPEC, EHEC, and *C. rodentium* induce diarrheal illness in part by injecting the highly conserved virulence factor EspF into enterocytes via type III secretion.<sup>50</sup> Although EspF has been shown to be a key mediator of AE pathogen-induced disruption of the intestinal barrier, the mechanism of EspF-dependent effects on the AJC is largely unknown. Because we found that N-WASP plays a role in the homeostatic maintenance of AJCs, and EspF has been shown to directly bind and activate N-WASP with high affinity,<sup>12</sup> we reasoned that EspF might act on the intercellular junction through an N-WASP-dependent pathway. Indeed, we found that N-WASP-depleted cells were resistant to EPEC-induced loss of barrier integrity in vitro. Because N-WASP also has been shown to play a role in facilitating the translocation of bacterial effector proteins by EHEC,<sup>51</sup> we considered whether the lack of junction disruption might be owing to ineffective type III secretion and impaired delivery of EspF. Several pieces of data indicate that translocation abnormalities in NWKD cells are unlikely to account for the failure of EspF-mediated barrier disruption. First, NWKD cells supported EPEC-induced actin pedestal formation, which is

dependent on Tir translocation.<sup>52</sup> We acknowledge that the finding of actin pedestals on EPEC-infected NWKD Caco-2 cells, but not during *C. rodentium* infection in mice, was somewhat unexpected. We suspect that given the central importance of Tir translocation and formation of the actin pedestal formation, AE pathogens have optimized mechanisms for recruiting and using even low levels of N-WASP protein, which may be present in the knockdown cells, but not in the epithelium of genetically depleted mice. In addition, ectopic expression of a WT EspF:green fluorescent protein (GFP) reporter construct induced strong cytoplasmic relocalization of TJ proteins in transfected WT, but not NWKD, cells (data not shown). Mutating N-WASP (or SNX9) binding sites in EspF, which is not predicted to affect EspF translocation, impaired the ability of EspF to induce TJ disruption in WT cells, which resembled the impairment seen in NWKD cells infected with EPEC expressing WT EspF. Taken together, these data show that EspF-induced tight junction disruption is mediated through N-WASP.

In addition to EspF/N-WASP interactions, we found that EspF also must bind SNX9 to disrupt the AJC. Previous studies have shown that an EPEC $\Delta$ espF strain expressing SNX9-binding-deficient mutant EspF could disrupt TER in polarized T84 cells,<sup>12</sup> suggesting that the ability to interact with SNX9 may be dispensable for EPEC-induced junction disruption. However, more recent work by Tapia et al<sup>53</sup> showed that EPEC EspF disrupts epithelial polarity, induces endocytosis, redistributes Na<sup>+</sup>/K<sup>+</sup> adenosine triphosphatase, and disrupts TJs by displacing Crumbs (Crb)3 from the Crb polarity complex of Crb3/Pals1/Patj. In these studies, the ability of EspF to induce mislocalization of Crb3 was abolished by either blocking the interaction of EspF/SNX9 or inhibiting the guanosine triphosphatase activity of dynamin. We found that SNX9-depleted Caco-2 cells were resistant to EPEC-induced loss of TER and that EPEC $\Delta$ espF transcomplemented with SNX9-binding-defective EspF failed to disrupt TER and AJC morphology. These discrepant results may be owing to differences in the expression of SNX9 and other closely related sorting nexins in different colon cancer cell lines.<sup>54–56</sup> Collectively, our findings show that EspF is similarly dependent on SNX9 and N-WASP to mediate EPEC-induced TJ alterations.

In vivo, EspF binding to either N-WASP or SNX9 appeared to play an important role in pathogen-induced weight loss (Figure 5B). Other investigators<sup>57,58</sup> have reported a modest degree of weight loss during CR infection, and we speculate that this may be owing to several factors. First, CR expressing WT EspF induced significant AJC disruption, which is associated with increased enteric fluid and electrolyte loss. In addition, although CR complemented with either N-WASP- or SNX9-binding-defective EspF showed high levels of colonization by day 7 of infection, stool recovery of these mutant strains was 1–2 logs lower than levels observed in mice infected with CR expressing native EspF. Differences in bacterial burden, reflecting enhanced pathogenicity of CR expressing nonvariant EspF, also may contribute to significant weight loss through changes in the underlying microbiota.<sup>59,60</sup>

The current work highlights the dual role that the master cytoskeletal regulator N-WASP plays in dynamic AJC assembly and disassembly. Further work will be required to determine how N-WASP facilitates the delivery and removal of specific TJ components to maintain intestinal homeostasis. A common theme in host–pathogen interactions is the utilization of otherwise homeostatic cell processes by invading microbes to enhance their pathogenesis. Consistent with the requirement of N-WASP for optimal junction plasticity and stability, we also found that EspF, an SNX9 interactor and direct inducer of N-WASP-dependent actin polymerization,<sup>12</sup> requires both N-WASP and SNX9 for efficient junction disruption. Although EspF has been shown previously to bind to both N-WASP and SNX9, we show, both in vitro and in vivo, that this binding is required for AE pathogens to induce intestinal barrier dysfunction. In addition to EPEC, EHEC, and *C. rodentium*, numerous microbes manipulate the host cytoskeletal machinery including the clinically important species *Helicobacter pylori* (associated with gastric ulcers and cancer),<sup>61,62</sup> adherent-invasive *E. coli* (associated with Crohn's disease),<sup>63</sup> and segmented filamentous bacteria (a potent inducer of Th17 immune responses).<sup>64</sup> By understanding the functions of N-WASP, and cytoskeletal regulation more generally, additional insight will be gained into host cell processes that are critical for cellular homeostasis as well as targets for many important human pathogens.

## References

1. Ivanov AI, McCall IC, Parkos CA, Nusrat A. Role for actin filament turnover and a myosin II motor in cytoskeleton-driven disassembly of the epithelial apical junctional complex. *Mol Biol Cell* 2004;15:2639–2651.
2. Mitic LL, Anderson JM. Molecular architecture of tight junctions. *Annu Rev Physiol* 1998;60:121–142.
3. Shen L, Turner JR. Actin depolymerization disrupts tight junctions via caveolae-mediated endocytosis. *Mol Biol Cell* 2005;16:3919–3936.
4. Kovacs EM, Verma S, Ali RG, Ratheesh A, Hamilton NA, Akhmanova A, Yap AS. N-WASP regulates the epithelial junctional actin cytoskeleton through a non-canonical post-nucleation pathway. *Nat Cell Biol* 2011;13:934–943.
5. Ivanov AI, Hunt D, Utech M, Nusrat A, Parkos CA. Differential roles for actin polymerization and a myosin II motor in assembly of the epithelial apical junctional complex. *Mol Biol Cell* 2005;16:2636–2650.
6. Otani T, Ichii T, Aono S, Takeichi M. Cdc42 GEF Tuba regulates the junctional configuration of simple epithelial cells. *J Cell Biol* 2006;175:135–146.
7. Georgiou M, Marinari E, Burden J, Baum B. Cdc42, Par6, and aPKC regulate Arp2/3-mediated endocytosis to control local adherens junction stability. *Curr Biol* 2008;18:1631–1638.
8. Leibfried A, Fricke R, Morgan MJ, Bogdan S, Bellaiche Y. *Drosophila* Cip4 and WASp define a branch of the Cdc42-Par6-aPKC pathway regulating E-cadherin endocytosis. *Curr Biol* 2008;18:1639–1648.
9. Guttman JA, Li Y, Wickham ME, Deng W, Vogl AW, Finlay BB. Attaching and effacing pathogen-induced

- tight junction disruption in vivo. *Cell Microbiol* 2006; 8:634–645.
10. Ma C, Wickham ME, Guttman JA, Deng W, Walker J, Madsen KL, Jacobson K, Vogl WA, Finlay BB, Vallance BA. *Citrobacter rodentium* infection causes both mitochondrial dysfunction and intestinal epithelial barrier disruption in vivo: role of mitochondrial associated protein (Map). *Cell Microbiol* 2006;8:1669–1686.
  11. Lommel S, Benesch S, Rohde M, Wehland J, Rottner K. Enterohaemorrhagic and enteropathogenic *Escherichia coli* use different mechanisms for actin pedestal formation that converge on N-WASP. *Cell Microbiol* 2004; 6:243–254.
  12. Alto NM, Weflen AW, Rardin MJ, Yarar D, Lazar CS, Tonikian R, Koller A, Taylor SS, Boone C, Sidhu SS, Schmid SL, Hecht GA, Dixon JE. The type III effector EspF coordinates membrane trafficking by the spatio-temporal activation of two eukaryotic signaling pathways. *J Cell Biol* 2007;178:1265–1278.
  13. van Weering JR, Sessions RB, Traer CJ, Kloer DP, Bhatia VK, Stamou D, Carlsson SR, Hurley JH, Cullen PJ. Molecular basis for SNX-BAR-mediated assembly of distinct endosomal sorting tubules. *EMBO J* 2012; 31:4466–4480.
  14. Worby CA, Dixon JE. Sorting out the cellular functions of sorting nexins. *Nat Rev Mol Cell Biol* 2002;3:919–931.
  15. el Marjou F, Janssen KP, Chang BH, Li M, Hindie V, Chan L, Louvard D, Chambon P, Metzger D, Robine S. Tissue-specific and inducible Cre-mediated recombination in the gut epithelium. *Genesis* 2004;39:186–193.
  16. Whitehead RH, Robinson PS. Establishment of conditionally immortalized epithelial cell lines from the intestinal tissue of adult normal and transgenic mice. *Am J Physiol Gastrointest Liver Physiol* 2009;296:G455–G460.
  17. Napolitano LM, Koruda MJ, Meyer AA, Baker CC. The impact of femur fracture with associated soft tissue injury on immune function and intestinal permeability. *Shock* 1996;5:202–207.
  18. Cerejido M, Gonzalez-Mariscal L, Contreras RG, Gallardo JM, Garcia-Villegas R, Valdes J. The making of a tight junction. *J Cell Sci Suppl* 1993;17:127–132.
  19. Diamond JM. Twenty-first Bowditch lecture. The epithelial junction: bridge, gate, and fence. *Physiologist* 1977;20:10–18.
  20. Wegener J, Sieber M, Galla HJ. Impedance analysis of epithelial and endothelial cell monolayers cultured on gold surfaces. *J Biochem Biophys Methods* 1996; 32:151–170.
  21. Miyoshi H, Stappenbeck TS. In vitro expansion and genetic modification of gastrointestinal stem cells in spheroid culture. *Nat Protoc* 2013;8:2471–2482.
  22. Clayburgh DR, Barrett TA, Tang Y, Meddings JB, Van Eldik LJ, Watterson DM, Clarke LL, Mrsny RJ, Turner JR. Epithelial myosin light chain kinase-dependent barrier dysfunction mediates T cell activation-induced diarrhea in vivo. *J Clin Invest* 2005;115:2702–2715.
  23. Gumbiner B, Simons K. A functional assay for proteins involved in establishing an epithelial occluding barrier: identification of a uvomorulin-like polypeptide. *J Cell Biol* 1986;102:457–468.
  24. Levine MM, Nataro JP, Karch H, Baldini MM, Kaper JB, Black RE, Clements ML, O'Brien AD. The diarrheal response of humans to some classic serotypes of enteropathogenic *Escherichia coli* is dependent on a plasmid encoding an enteroadhesiveness factor. *J Infect Dis* 1985;152:550–559.
  25. McNamara BP, Donnenberg MS. A novel proline-rich protein, EspF, is secreted from enteropathogenic *Escherichia coli* via the type III export pathway. *FEMS Microbiol Lett* 1998;166:71–78.
  26. Datsenko KA, Wanner BL. One-step inactivation of chromosomal genes in *Escherichia coli* K-12 using PCR products. *Proc Natl Acad Sci U S A* 2000; 97:6640–6645.
  27. Nougayrede JP, Donnenberg MS. Enteropathogenic *Escherichia coli* EspF is targeted to mitochondria and is required to initiate the mitochondrial death pathway. *Cell Microbiol* 2004;6:1097–1111.
  28. Cheng HC, Skehan BM, Campellone KG, Leong JM, Rosen MK. Structural mechanism of WASP activation by the enterohaemorrhagic *E. coli* effector EspF(U). *Nature* 2008;454:1009–1013.
  29. Snapper CM, Shen Y, Khan AQ, Colino J, Zelazowski P, Mond JJ, Gause WC, Wu ZQ. Distinct types of T-cell help for the induction of a humoral immune response to *Streptococcus pneumoniae*. *Trends Immunol* 2001; 22:308–311.
  30. Cotta-de-Almeida V, Westerberg L, Maillard MH, Onaldi D, Wachtel H, Meelu P, Chung UI, Xavier R, Alt FW, Snapper SB. Wiskott Aldrich syndrome protein (WASP) and N-WASP are critical for T cell development. *Proc Natl Acad Sci U S A* 2007;104:15424–15429.
  31. Lyubimova A, Garber JJ, Upadhyay G, Sharov A, Anastasoie F, Yajnik V, Cotsarelis G, Dotto GP, Botchkarev V, Snapper SB. Neural Wiskott-Aldrich syndrome protein modulates Wnt signaling and is required for hair follicle cycling in mice. *J Clin Invest* 2010; 120:446–456.
  32. Mallick EM, Garber JJ, Vanguri VK, Balasubramanian S, Blood T, Clark S, Vingadassalom D, Louissaint C, McCormick B, Snapper SB, Leong JM. The ability of an attaching and effacing pathogen to trigger localized actin assembly contributes to virulence by promoting mucosal attachment. *Cell Microbiol* 2014;16: 1405–1424.
  33. Smutny M, Cox HL, Leerberg JM, Kovacs EM, Conti MA, Ferguson C, Hamilton NA, Parton RG, Adelstein RS, Yap AS. Myosin II isoforms identify distinct functional modules that support integrity of the epithelial zonula adherens. *Nat Cell Biol* 2010;12:696–702.
  34. Kalman D, Weiner OD, Goosney DL, Sedat JW, Finlay BB, Abo A, Bishop JM. Enteropathogenic *E. coli* acts through WASP and Arp2/3 complex to form actin pedestals. *Nat Cell Biol* 1999;1:389–391.
  35. Crepin VF, Girard F, Schuller S, Phillips AD, Mousnier A, Frankel G. Dissecting the role of the Tir:Nck and Tir:IRTKS/IRSp53 signalling pathways in vivo. *Mol Microbiol* 2010;75:308–323.
  36. Luperchio SA, Newman JV, Dangler CA, Schrenzel MD, Brenner DJ, Steigerwalt AG, Schauer DB. *Citrobacter*



- rodentium, the causative agent of transmissible murine colonic hyperplasia, exhibits clonality: synonymy of *C. rodentium* and mouse-pathogenic *Escherichia coli*. *J Clin Microbiol* 2000;38:4343–4350.
37. Schauer DB, Falkow S. The *eae* gene of *Citrobacter freundii* biotype 4280 is necessary for colonization in transmissible murine colonic hyperplasia. *Infect Immun* 1993;61:4654–4661.
  38. Zhou K, Sumigray KD, Lechler T. The Arp2/3 complex has essential roles in vesicle trafficking and transcytosis in the mammalian small intestine. *Mol Biol Cell* 2015;26:1995–2004.
  39. Attar N, Cullen PJ. The retromer complex. *Adv Enzyme Regul* 2010;50:216–236.
  40. Bonifacino JS, Hurley JH. Retromer. *Curr Opin Cell Biol* 2008;20:427–436.
  41. Collins BM. The structure and function of the retromer protein complex. *Traffic* 2008;9:1811–1822.
  42. Citalan-Madrid AF, Vargas-Robles H, Garcia-Ponce A, Shibayama M, Betanzos A, Nava P, Salinas-Lara C, Rottner K, Mennigen R, Schnoor M. Cortactin deficiency causes increased RhoA/ROCK1-dependent actomyosin contractility, intestinal epithelial barrier dysfunction, and disproportionately severe DSS-induced colitis. *Mucosal Immunol* 2017;10:1237–1247.
  43. Goley ED, Welch MD. The ARP2/3 complex: an actin nucleator comes of age. *Nat Rev Mol Cell Biol* 2006;7:713–726.
  44. Mohri K, Ono K, Yu R, Yamashiro S, Ono S. Enhancement of actin-depolymerizing factor/cofilin-dependent actin disassembly by actin-interacting protein 1 is required for organized actin filament assembly in the *Caenorhabditis elegans* body wall muscle. *Mol Biol Cell* 2006;17:2190–2199.
  45. Nadkarni AV, Briehner WM. Aip1 destabilizes cofilin-saturated actin filaments by severing and accelerating monomer dissociation from ends. *Curr Biol* 2014;24:2749–2757.
  46. Okada K, Ravi H, Smith EM, Goode BL. Aip1 and cofilin promote rapid turnover of yeast actin patches and cables: a coordinated mechanism for severing and capping filaments. *Mol Biol Cell* 2006;17:2855–2868.
  47. Lechuga S, Baranwal S, Ivanov AI. Actin-interacting protein 1 controls assembly and permeability of intestinal epithelial apical junctions. *Am J Physiol Gastrointest Liver Physiol* 2015;308:G745–G756.
  48. Wang D, Naydenov NG, Feygin A, Baranwal S, Kuemmerle JF, Ivanov AI. Actin-depolymerizing factor and cofilin-1 have unique and overlapping functions in regulating intestinal epithelial junctions and mucosal inflammation. *Am J Pathol* 2016;186:844–858.
  49. Andrianantoandro E, Pollard TD. Mechanism of actin filament turnover by severing and nucleation at different concentrations of ADF/cofilin. *Mol Cell* 2006;24:13–23.
  50. Luperchio SA, Schauer DB. Molecular pathogenesis of *Citrobacter rodentium* and transmissible murine colonic hyperplasia. *Microbes Infect* 2001;3:333–340.
  51. Vingadassalom D, Campellone KG, Brady MJ, Skehan B, Battle SE, Robbins D, Kapoor A, Hecht G, Snapper SB, Leong JM. Enterohemorrhagic *E. coli* requires N-WASP for efficient type III translocation but not for EspFU-mediated actin pedestal formation. *PLoS Pathog* 2010;6:e1001056.
  52. Campellone KG, Rankin S, Pawson T, Kirschner MW, Tipper DJ, Leong JM. Clustering of Nck by a 12-residue Tir phosphopeptide is sufficient to trigger localized actin assembly. *J Cell Biol* 2004;164:407–416.
  53. Tapia R, Kralicek SE, Hecht GA. EPEC effector EspF promotes Crumbs3 endocytosis and disrupts epithelial cell polarity. *Cell Microbiol* 2017;19(11). <https://doi.org/10.1111/cmi.12757>, Epub 2017 Jul 27.
  54. Zhang J, Zhang X, Guo Y, Xu L, Pei D. Sorting nexin 33 induces mammalian cell micronucleated phenotype and actin polymerization by interacting with Wiskott-Aldrich syndrome protein. *J Biol Chem* 2009;284:21659–21669.
  55. Park J, Kim Y, Lee S, Park JJ, Park ZY, Sun W, Kim H, Chang S. SNX18 shares a redundant role with SNX9 and modulates endocytic trafficking at the plasma membrane. *J Cell Sci* 2010;123:1742–1750.
  56. Haberg K, Lundmark R, Carlsson SR. SNX18 is an SNX9 paralog that acts as a membrane tubulator in AP-1-positive endosomal trafficking. *J Cell Sci* 2008;121:1495–1505.
  57. Bhinder G, Sham HP, Chan JM, Morampudi V, Jacobson K, Vallance BA. The *Citrobacter rodentium* mouse model: studying pathogen and host contributions to infectious colitis. *J Vis Exp* 2013;72:e50222.
  58. Vijayakumar V, Santiago A, Smith R, Smith M, Robins-Browne RM, Nataro JP, Ruiz-Perez F. Role of class 1 serine protease autotransporter in the pathogenesis of *Citrobacter rodentium* colitis. *Infect Immun* 2014;82:2626–2636.
  59. Lupp C, Robertson ML, Wickham ME, Sekirov I, Champion OL, Gaynor EC, Finlay BB. Host-mediated inflammation disrupts the intestinal microbiota and promotes the overgrowth of Enterobacteriaceae. *Cell Host Microbe* 2007;2:204.
  60. Wickham ME, Brown NF, Boyle EC, Coombes BK, Finlay BB. Virulence is positively selected by transmission success between mammalian hosts. *Curr Biol* 2007;17:783–788.
  61. Su B, Ceponis PJ, Sherman PM. Cytoskeletal rearrangements in gastric epithelial cells in response to *Helicobacter pylori* infection. *J Med Microbiol* 2003;52:861–867.
  62. Tabassam FH, Graham DY, Yamaoka Y. OipA plays a role in *Helicobacter pylori*-induced focal adhesion kinase activation and cytoskeletal re-organization. *Cell Microbiol* 2008;10:1008–1020.
  63. Darfeuille-Michaud A, Boudeau J, Bulois P, Neut C, Glasser AL, Barnich N, Bringer MA, Swidsinski A, Beaugerie L, Colombel JF. High prevalence of adherent-invasive *Escherichia coli* associated with ileal mucosa in Crohn's disease. *Gastroenterology* 2004;127:412–421.
  64. Ivanov II, Atarashi K, Manel N, Brodie EL, Shima T, Karaoz U, Wei D, Goldfarb KC, Santee CA, Lynch SV, Tanoue T, Imaoka A, Itoh K, Takeda K, Umesaki Y, Honda K, Littman DR. Induction of intestinal Th17 cells by segmented filamentous bacteria. *Cell* 2009;139:485–498.

---

Received April 14, 2017. Accepted November 28, 2017.

**Correspondence**

Address correspondence to: Scott B. Snapper, MD, PhD, Division of Gastroenterology/Nutrition, Boston Children's Hospital, Enders 676, 300 Longwood Avenue, Boston, Massachusetts 02115. e-mail: [Scott.Snapper@childrens.harvard.edu](mailto:Scott.Snapper@childrens.harvard.edu); fax: (617) 730-0498.

**Acknowledgments**

The authors thank our laboratory colleagues for their advice and support and other colleagues for the gifts of reagents, notably M. Kirschner (Harvard Medical School) for an early gift of N-WASP antibodies. Special thanks to Timothy Blood who constructed the *C rodentium*Δ*espF* mutant while in the Leong Laboratory (Boston, MA) and to Tracy Mandichak, who made the modular EspF plasmids while in the Donnenberg Laboratory (Baltimore, MD).

Present address for Michael S. Donnenberg: Departments of Medicine, Microbiology & Immunology and Biochemistry & Molecular Biology, Virginia Commonwealth University, Richmond, Virginia.

**Author contributions**

John Garber was responsible for the study concept and design, acquisition, analysis, and interpretation of data, and drafting the manuscript; Emily Mallick

and Karen Scanlon were responsible for the acquisition and analysis of data; Jerrold Turner was responsible for the analysis and interpretation of data, and critical revision of the manuscript for important intellectual content; Michael Donnenberg was responsible for the analysis and interpretation of data, and critical revision of the manuscript for important intellectual content; John Leong was responsible for the study concept and design, analysis and interpretation of data, and critical revision of the manuscript for important intellectual content; and Scott Snapper was responsible for the study concept and design, interpretation of data, drafting the manuscript, and study supervision.

**Conflicts of interest**

The authors disclose no conflicts.

**Funding**

This work was financially supported by National Institute of Health grants K08 DK094966 (J.J.G.), P01 HL059561 (S.B.S.), and R01 AI46454 (J.M.L.), as well as the generous support of the Crohn's and Colitis Foundation of America in the form of a Career Development Award (J.J.G.) and a Senior Research Award (S.B.S.). Confocal imaging was performed at the Advanced Imaging Core of the Harvard Digestive Diseases Center, which is supported by National Institutes of Health grant P30 DK034854.